

# Preserving Localized Patch Semantics in VLMs

Parsa Esmaeilkhani<sup>1</sup> Longin Jan Latecki<sup>1</sup>

## Abstract

Logit Lens has been proposed for visualizing tokens that contribute most to the LLM answers. Recently, Logit Lens was also shown to be applicable in autoregressive Vision-Language Models (VLMs), where it illustrates the conceptual content of image tokens in the form of heatmaps, e.g., which image tokens are likely to depict the concept of cat in a given image. However, the visual content of image tokens often gets diffused to language tokens, and consequently, the locality of visual information gets mostly destroyed, which renders Logit Lens’s visualization unusable for explainability. To address this issue, we introduce a complementary loss to the next-token prediction (NTP) to prevent the visual tokens from losing visual representation inherited from corresponding image patches. The proposed Logit Lens Loss (LLL) is designed to make visual token embeddings more semantically aligned with the textual concepts that describe their image regions (e.g., patches containing a cat with the word “cat”), without requiring any architectural modification or large-scale training. This way LLL constraints the mixing of image and text tokens in the self-attention layers in order to prevent image tokens from losing their localized visual information. As our experiments show, LLL not only makes Logit Lens practically relevant by producing meaningful object confidence maps in images, but also improves performance on vision-centric tasks like segmentation without attaching any special heads.

## 1. Introduction

We focus on autoregressive Vision-Language Models (VLMs) like Llava (Liu et al., 2023), MiniGPT4 (Zhu et al., 2023), and Qwen-VL (Bai et al., 2023). Fig. 1 illustrates their processing flow. The input image (or images)

<sup>1</sup> Department of Computer and Information Sciences, Temple University, Philadelphia, USA. Correspondence to: Parsa Esmaeilkhani <parsa.esmaeilkhani@temple.edu>, Longin Jan Latecki <latecki@temple.edu>.

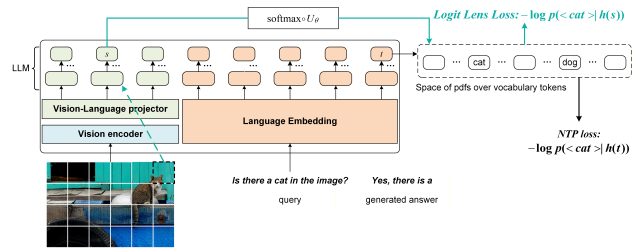


Figure 1. VLM components with the added Logit Lens Loss (LLL) shown in cyan. While NTP loss maximizes the probability of generating ground truth text tokens, LLL increases the probability of visual tokens  $s$  to predict text tokens describing their content, e.g., if visual token  $s$  represents a patch containing part of a cat, the probability of predicting token  $<\text{cat}>$  is increased. This way LLL maximizes the alignment of deep embeddings of image patches containing the cat with text token  $<\text{cat}>$ .

is first passed through a frozen visual encoder (typically a ViT, CLIP, or DINOv2) to extract image tokens and map them into a language embedding space with a linear projection module. Subsequently, the mapped image tokens, often called visual tokens, are used as part of the LLM input, along with the text input (and special tokens). As visual tokens are transformed through the layers of an LLM, their embeddings change. In particular, the embeddings of visual tokens are mixed with the embeddings of language tokens in the attention layers of the LLM module. However, there is a risk that information carried by visual tokens becomes diluted among the predominantly textual tokens as they propagate through the LLM layers. In particular, the information of visual tokens may be transferred to language tokens, as nicely demonstrated in (Kaduri et al., 2025). In an extreme case, the visual tokens are ignored, and the LLM can even hallucinate an image description for an empty image, as was demonstrated in (Liu et al., 2024; Tong et al., 2024). Further evidence that visual tokens are often ignored among all LLM tokens is the fact that after removing half of the visual tokens, the VLM performance does not decrease (Chen et al., 2024). An unintended consequence is that the connection of visual tokens to the content of corresponding image regions is lost in this process. As pointed out in (Fu et al., 2025), *The LLM’s ability to use its vision representations is a limiting factor in VLM performance*.

We aim to address this issue by constraining the mixing of visual and language tokens in order to prevent

**the modality mixing from degrading visual information.**

This uncontrolled modality mixing often causes visual embeddings to lose their direct correspondence to the image regions from which they originated. Consequently, visual tokens may no longer encode the localized, semantic content of their source patches. Our main contribution is a **novel visual grounding loss applied directly to visual tokens** to maintain semantic alignment with the language concepts describing their image regions, even after transformation through the LLM attention layers.

The key idea of the proposed loss is to increase the association of each visual token with the language concepts describing its content. For example, if a given image patch contains part of a cat, its visual token should yield a high probability of the vocabulary token  $< cat >$ . To formulate this idea, we map deep embeddings of visual tokens to probability distributions (pdf) over language vocabulary tokens to recover textual semantics directly from visual embeddings, see Fig. 1. Here we utilize Logit Lens (nostalgia**braist**, 2020) that was originally proposed for LLMs. Logit Lens demonstrated that mapping of a deep embedding to the pdf space is not only useful for the next-token prediction when applied to the deep embedding of the previous token, but can also reveal the content of other LLM tokens. As shown in (Jiang et al., 2025), Logit Lens provides insight into the representation of visual tokens in VLMs as well. If we focus on a selected text token, e.g.,  $< cat >$ , Logit Lens enables us to generate object confidence (or localization) maps over the input image, showing for each patch how strongly it is associated with the selected token. However, the Logit Lens visualization does not work well, in particular, if one moves away from LLava, used in (Jiang et al., 2025), to newer VLMs like Qwen2.5-VL, as demonstrated in Fig. 2. The reason is the diffusion of localized image information away from visual to text tokens.

To address this issue, and hence make Logit Lens visualization work in VLMs, we propose to utilize the Logit Lens object confidence maps as a tool for visual grounding of VLMs. We achieve this with a new loss function called **Logit Lens Loss (LLL)**. LLL allows us to increase the alignment between deep visual patch embeddings and language tokens inside a VLM by utilizing the latent language semantics of each image patch. In our framework, the space of probability distributions over the vocabulary tokens is used to link visual and text tokens, since both types of tokens can be mapped to this space as graphically illustrated with cyan lines in Fig. 1. While NTP loss increases the probability of generating a particular vocabulary token, e.g.,  $< cat >$ , conditioned on previously generated text tokens, LLL increases the probability of  $< cat >$  conditioned on visual tokens representing patches containing the cat in a given image. Consequently, the deep embeddings of these patches become more aligned with the deep embedding of

$< cat >$ .

Our approach differs from the majority of visual grounding works in that it intrinsically links visual and text tokens by making their deep embeddings more aligned, while works like (Peng et al., 2023; Rasheed et al., 2024; Lai et al., 2024; Wu et al., 2025b) use the LLM predictions (or VLM external modules) to predict object locations as bounding box (BB) coordinates or as segmentation masks. In these works, the LLM backbone of a VLM predicts BB coordinates without directly linking them to actual visual patches containing the target object. So, this can be illustrated as:

$$[\text{image} + \text{text}] \rightarrow \text{LLM} \rightarrow [\text{text} + \text{BB as text}].$$

For example, for a query "Where is a cat in the image?", a VLM can generate correct BB coordinates (as text) without knowing the image tokens containing the cat. Of course, we can use a deterministic algorithm to draw the BB on top of the image, as it is commonly done, but the VLM is not intrinsically aware of which image patches contain the cat. Encoding this intrinsic awareness into deep embeddings of visual tokens is the driving motivation of the proposed LLL.

Our main contributions can be summarized as follows:

- **Introduce a novel visual grounding loss (Logit Lens Loss, LLL):** A new loss is applied directly to visual tokens to preserve their connection to the underlying image content as they propagate through LLM layers. LLL constrains cross-modal mixing in the LLM attention layers, and consequently, it mitigates uncontrolled mixing of visual and text tokens, helping visual tokens to retain visual information.
- **Embed intrinsic localization within the VLM:** Unlike prior work that predicts bounding boxes or masks without binding predictions to specific image patches, the proposed LLL explicitly links semantic concepts to the visual tokens that represent their true spatial locations without any architectural modifications. We visualize this with object confidence maps.
- **Increased interpretability of Logit Lens in VLM:** As our experimental results demonstrate, LLL makes Logit Lens visualization in the form of object confidence maps a useful tool for VLM explainability. The maps a few orders of magnitude better than those generated by baseline VLMs and ones finetuned with NTP only. Moreover, also significantly increases the attention of answer tokens to relevant image regions.

Overall, LLL is designed to make visual token embeddings more semantically aligned with the textual concepts that describe their image regions, without requiring any architectural modification or large-scale training. Our goal is to demonstrate the effect of grounding visual embeddings

directly in the vocabulary space, enabling stronger visual–language alignment within standard VLM backbones. Although we use bounding boxes as lightweight supervision to indicate which visual tokens correspond to an object during training, LLL does not introduce any detection heads or localization modules, and the original VLM architecture remains unchanged. This separates our approach from prior work and is clearly reflected in the object confidence maps shown in Fig. 2, where LLL produces significantly more accurate and interpretable localization signals.

We do not intend to teach VLMs new concepts but to preserve their localized image understanding, and consequently, make Logit Lens visualisation useful in VLM explainability. We focus on finetuning, even though the proposed LLL could be applied in pre-training, it is beyond the scope of this paper.

## 2. Preliminaries

### 2.1. Vision-Language Models

The architecture of recent autoregressive VLMs for text generation typically involves three main components: a vision encoder to process image inputs, a mapping network to project image features into image embeddings, and an autoregressive language model to process both image and prompt embeddings to generate text. We focus on two recent state-of-the-art VLMs: LLava-v1.5 (Liu et al., 2023) and Qwen2.5-VL (Bai et al., 2025), both used in their 7B-parameter versions. LLava-v1.5 uses a frozen CLIP vision encoder and an MLP projection head trained on vision-language data, followed by instruction tuning. In contrast, Qwen2.5-VL employs a jointly trained vision-language architecture in which the vision encoder and projection layers are co-optimized with the language model.

The VLM input sequence typically includes visual tokens  $\mathcal{P}$  from the image, followed by text tokens  $\mathcal{T}$  for instructions. These segments are concatenated to form the full input context:  $\mathbf{X} = [\mathcal{P}, \mathcal{T}]$ . All of the visual and language tokens are passed through the LLM backbone and mixed by the attention layers in a joint embedding space, which is language-dominated (Wang et al., 2024), since LLMs are pretrained on a huge amount of text data. The LLM then generates an answer sequence  $\mathcal{A} = (t_1, \dots, t_{|\mathcal{A}|})$  token-by-token under a left-to-right causal mask.

During generation, at each step  $i$ , the model attends only to tokens at positions  $< i$  and selects the most probable next token from its vocabulary. More precisely, an unembedding matrix  $U_\theta \in \mathbb{R}^{|\mathcal{V}| \times d}$  maps the latent representation  $h_L(t_{i-1})$  of token  $t_{i-1}$  to a probability distribution over the vocabulary  $\mathcal{V}$  for the prediction of next token  $t_i$ , where  $h_L(t_{i-1}) \in \mathbb{R}^d$  is obtained by transforming the previously generated token  $t_{i-1}$  through layers 1 to  $L$  of the LLM backbone. So, at each step  $i$  the model predicts  $t_i$  conditioned

on the full context  $\mathbf{X}$  and the previously generated answer tokens  $\mathcal{A}_{a < i} = (t_1, \dots, t_{i-1})$ .

During VLM training, the standard next-token prediction (NTP) loss is used:

$$L_{\text{NTP}}(\theta) = \frac{1}{|\mathcal{A}|} \sum_{i=1}^{|\mathcal{A}|} -\log p_\theta(t_i \mid \mathcal{A}_{a < i}, \mathbf{X}) \quad (1)$$

where  $p_\theta(t_i \mid \mathcal{A}_{a < i}, \mathbf{X}) = p_\theta(t_i \mid h_L(t_{i-1}))$  is the probability of generating the next ground truth token  $t_i \in \mathcal{V}$ ,  $\theta$  denotes the model parameters, and  $|\mathcal{A}|$  is the length of the answer sequence. We observe that the NTP loss does not include any incentives for preserving the image content initially encoded in visual tokens  $\mathcal{P}$ .

### 2.2. Logit Lens

We use the Logit Lens (Jiang et al., 2025) to reveal how visual tokens evolve into textual concepts within a VLM. Originally designed to analyze intermediate representations in language models, Logit Lens (nostalgiaibrist, 2020) offers a direct way to project latent embeddings into the LLM’s vocabulary space. It takes an embedding  $h_l(x) \in \mathbb{R}^d$  at any LLM layer and projects it through the model’s unembedding matrix  $U_\theta : \mathbb{R}^d \rightarrow \mathbb{R}^{\mathcal{V}}$ , which is the same matrix as used at the final LLM layer to predict vocabulary logits. This gives us a logit vector over the vocabulary of text tokens:

$$U_\theta h_l(x) = [\text{logit}_1, \text{logit}_2, \dots, \text{logit}_{|\mathcal{V}|}], \quad (2)$$

where  $\text{logit}_j$  corresponds to token  $j$  in the vocabulary  $\mathcal{V}$ . This vector represents the model’s predicted logit distribution over tokens after layer  $l$ .

Given the logits vector obtained from the matrix-vector multiplication  $U_\theta h_l(x)$ , the probability distribution over the vocabulary is computed using the softmax function:

$$p_\theta(v_j \mid h_l(x)) = \frac{\exp(\text{logit}_j)}{\sum_{k=1}^{|\mathcal{V}|} \exp(\text{logit}_k)}, \quad \forall v_j \in \mathcal{V}. \quad (3)$$

This yields the model’s predicted token probabilities at layer  $l$ , where  $p_\theta(v_j \mid h_l(x))$  denotes the probability of token  $v_j$  conditioned on the latent representation  $h_l(x)$ .

When applied to a visual token  $x = s_i$ , the resulting probability vector  $p_\theta(v_j \mid h_l(s_i))$  represents the distribution over vocabulary tokens that describes the visual content of patch  $i$  as perceived by the model with parameter  $\theta$  at layer  $l$ . This allows us to identify which word tokens, e.g., “cat”, “bottle”, the model associates most strongly with each patch. So, using the Logit Lens on visual tokens directly relates the corresponding image patches to textual concepts.

## 3. Methodology: Logit Lens Loss

As our confidence maps demonstrate in Fig. 2, VLMs only partially focus on the correct image patches corresponding

to an object category. This occurs because VLMs finetuned with next-token prediction receive only weak supervision regarding the visual patterns present in the image. This observation motivates us to explore how to teach VLMs to ensure that visual tokens remain semantically tied to the image regions they represent as they propagate through the language model layers, without sacrificing the language modeling capabilities of the LLM component.

While NTP optimizes the model for textual coherence, it does not directly constrain the internal representations of visual tokens, allowing them to drift away from their image-related content as attention layers mix visual and textual embeddings. To address this, we introduce a grounding objective that explicitly links each visual token to the textual concepts describing its underlying image content.

Our approach builds on the idea that every deep embedding  $h_l(x)$  within the LLM implicitly encodes a distribution over vocabulary tokens via the Logit Lens projection  $U_\theta h_l(x)$ . By treating this distribution as the “semantic fingerprint” of a patch, we define a loss that encourages visual tokens corresponding to object regions to produce vocabulary distributions consistent with their ground-truth labels (e.g., high probability for the word “cat” inside a cat region, and low elsewhere). Meanwhile, the loss discourages patches unrelated to a given object category from developing unrelated connections with that category. In essence, it drives each patch to focus more on objects present within its region and less on those absent. This yields a simple yet effective auxiliary objective, termed Logit Lens Loss, that complements the standard NTP loss by grounding visual embeddings directly in the vocabulary space.

Let  $\mathcal{P}$  denote the set of all visual (patch) tokens in the image and  $\mathcal{P}' \subseteq \mathcal{P}$  the subset of patches inside the ground-truth region (e.g., bounding box) of the queried object (when present). In other words, we obtain  $\mathcal{P}'$  by projecting the ground-truth bounding box onto the visual-token grid and selecting tokens whose receptive fields overlap with the annotated object region.

Following common practice in visual grounding tasks, we use bounding box annotations as supervision to indicate which visual tokens correspond to the target object during training (Xiao et al., 2024).

For a target vocabulary token  $v$  and layer- $l$  representation  $h_l(s)$ , **Logit Lens Loss (LLL)** is defined as

$$L_{\text{LLL}}(\theta) = \frac{1}{|\mathcal{P}'|} \sum_{s \in \mathcal{P}'} -\log p_\theta(v | h_l(s)) + \frac{1}{|\mathcal{P} \setminus \mathcal{P}'|} \sum_{s \in \mathcal{P} \setminus \mathcal{P}'} -\log (1 - p_\theta(v | h_l(s))) \quad (4)$$

When the queried concept spans multiple tokens (e.g., sub-

word splits or multi-word phrases), we use a token set  $V \subseteq \mathcal{V}$  and apply the loss to each token independently and average across tokens.

For simplicity, let’s say  $v = \{\text{< cat >}\}$  is a vocabulary token representing the word “cat” and  $\mathcal{P}'$  is a subset of visual tokens corresponding to image patches depicting the cat in the input image, then Eq. (4) reduces to

$$L_{\text{LLL}}(\theta) = \frac{1}{|\mathcal{P}'|} \sum_{s \in \mathcal{P}'} -\log p_\theta(\text{< cat >} | h_l(s)). \quad (5)$$

It aims at increasing the probability of token  $\text{< cat >}$  in the vocabulary distribution for each deep embedding  $h_l(s)$  of image patch  $s \in \mathcal{P}'$  that depicts the cat in the image. We stress that this does not suppress other concepts like “kitten” or “cat ear”. The expressive power of a VLM comes from its pre-training; the LLL only helps to preserve the image-grounded locality of visual deep embeddings, and does not aim at teaching new concepts to VLMs.

The second term in Eq. (4) aims at decreasing the probability of token  $\text{< cat >}$  in the vocabulary distribution for each deep embedding  $h_l(s)$  of image patch  $s \in \mathcal{P} \setminus \mathcal{P}'$  outside the cat bounding box.

We propose to use the  $L_{\text{LLL}}$  as the auxiliary loss in addition to the next token prediction loss  $L_{\text{NTP}}(\theta)$  of the VLM to optimize the VLM’s parameters for both objectives:

$$L_{\text{total}} = L_{\text{NTP}} + \lambda L_{\text{LLL}}. \quad (6)$$

We empirically set  $\lambda$  to 0.5, which we found effective across all tasks. Like  $L_{\text{NTP}}$ , the proposed  $L_{\text{LLL}}$  is only applied to the last VLM layer, i.e.,  $l = L$  in Eq. (4). Moreover, after finetuning with LLL, it is also sufficient to apply Logit Lens to the last layer. In contrast, in (Jiang et al., 2025), Logit Lens is computed as the maximum over all layers.

Both terms in Eq. (6) are nicely aligned since both are based on increasing the probabilities of generating selected vocabulary tokens, as illustrated in Fig. 1. Formally, since both visual and textual embeddings can be projected into probability distributions over the vocabulary via the Logit Lens, they share a common semantic space. We denote this shared space with  $\mathcal{F}$  of all probability distribution functions (pdfs)  $p_\theta(\cdot | h_l(x)) : \mathcal{V} \rightarrow [0, 1]$  over the vocabulary tokens  $\mathcal{V}$ , i.e.,

$$\mathcal{F} = \{p_\theta(\cdot | h_l(x)) \mid x \in \mathbb{R}^d\}. \quad (7)$$

Let  $f : \mathbb{R}^d \rightarrow \mathcal{F}$  be defined as  $f = \text{softmax} \circ U_\theta$  following the process in Sec. 2.2. Space  $\mathcal{F}$  is a common space to link the visual and language tokens, since  $f(s) \in \mathcal{F}$  and  $f(t) \in \mathcal{F}$  for all visual tokens  $s \in \mathcal{P}$  and text tokens  $t \in \mathcal{T}$ .

For example, if a given visual token  $s$  corresponds to an image patch containing part of a cat, we want  $p_\theta(\text{< cat >} | h_l(s))$  to have a high value, which is analogous to increasing

the probability of generating token  $t_i = \langle \text{cat} \rangle$  as the next ground truth token, which is given by  $p_\theta(t_i | \mathcal{A}_{a < i}, \mathbf{X}) = p_\theta(t_i | h_L(t_{i-1}))$  in the next-token prediction loss  $L_{\text{NTP}}$ .

LLL applies the loss directly to visual tokens, while NTP applies loss directly only at text positions. Minimizing  $L_{\text{LLL}}$  applies cross-entropy through the unembedding matrix to visual tokens, whose gradient explicitly pulls the patch embedding  $h_L(s)$  toward the unembedding vector of the target word  $v$ , thereby enforcing semantic alignment in the same space the LLM uses to generate language.

#### 4. Gradient Strength

We show that **the gradient of  $L_{\text{LLL}}$  provides a direct signal to visual tokens**. For simplicity, let us consider a single positive visual token  $\mathcal{P}' = \{s\}$  in the last layer  $L$ . Then  $L_{\text{LLL}}$  reduces to

$$\mathcal{L}_{\text{LLL}}(s) = -\log p_\theta(v | h_L(s)). \quad (8)$$

Let  $z = Uh_L(s)$ , where  $U$  is the unembedding matrix,  $p = \text{softmax}(z)$ , and  $p_v = p_\theta(v | h_L(s))$ . Using the standard softmax cross-entropy derivative,

$$\frac{\partial}{\partial z}(-\log p_v) = p - e_v, \quad (9)$$

where  $e_v$  is the one-hot vector for token  $v$  and vector  $p \in \mathbb{R}^{|V|}$  denotes the softmax probability distribution over the vocabulary:  $p = \text{softmax}(Uh_L(s))$ ,  $\sum_{j=1}^{|V|} p_j = 1$ . By the chain rule,

$$\frac{\partial \mathcal{L}_{\text{LLL}}(s)}{\partial h_L(s)} = U^\top(p - e_v) = \sum_j p_j U_j^\top - U_v^\top, \quad (10)$$

where scalar  $p_j$  is the  $j$ -th component of  $p$ , corresponding to the probability assigned to vocabulary token  $j$ .

We obtain that minimizing  $\mathcal{L}_{\text{LLL}}$  directly pushes the last-layer patch representation  $h_L(s)$  toward the unembedding direction corresponding to the target vocabulary token  $v$ .

**In contrast, the NTP provides only a weak signal to the majority of visual tokens**, as we show now. Since the gradient of NTP loss only flows directly to the previously generated text token, it can only flow to a visual token  $s$  through self-attention. However, most text tokens exhibit only weak attention to visual tokens. More formally, the NTP loss  $L_{\text{NTP}}$  is applied at the text output position, so the gradient at that position backpropagates through self-attention and cross-attention to  $h_L(s)$ . Formally,

$$\nabla_{h_L(s)} L_{\text{NTP}}(\theta) = \sum_{j \in \mathcal{T}} \underbrace{\nabla_{h_L(j)} L_{\text{NTP}}(\theta)}_{\text{local at text token}} \cdot \underbrace{\frac{\partial h_L(j)}{\partial h_L(s)}}_{\text{attention path}}, \quad (11)$$

where the NTP loss gradient is summed over text tokens  $\mathcal{T}$  because only text tokens receive the language-model

loss, since the language-model head is applied to them. The visual tokens do not get direct gradients from NTP, so they do not contribute to the chain rule, leaving cross-attention from text tokens as the only pathway by which NTP's gradient reaches a visual token.

At the final VLM layer, the dependence of a text token  $j$  on a visual token  $s$  arises through a cross-attention block. For such a block, the Jacobian of the hidden state satisfies

$$\left\| \frac{\partial h_L(j)}{\partial h_L(s)} \right\| \leq C_{\text{att}} a_{js}, \quad (12)$$

where  $a_{js}$  is the attention weight from text token  $j$  to visual token  $s$ , and  $C_{\text{att}}$  is a constant depending on the operator norms of the projection matrices ( $W_Q, W_K, W_V, W_O$ ) and the layer normalization. So, the Jacobian  $\partial h_L(j) / \partial h_L(s)$  is dominated by the attention weight  $a_{js}$  from token  $j$  to  $s$ , times bounded transformation matrices  $C_{\text{att}}$ .

Substituting Eq. (12) into Eq. (11) gives

$$\left\| \nabla_{h_L(s)} L_{\text{NTP}} \right\| \leq C_{\text{att}} \sum_{j \in \mathcal{T}} \left\| \nabla_{h_L(j)} L_{\text{NTP}} \right\| a_{js}. \quad (13)$$

$\left\| \nabla_{h_L(j)} L_{\text{NTP}} \right\|$  is capped by  $\sqrt{2} \|U\|$  for all  $j \in \mathcal{T}$  (ignoring any extra scaling tricks); so it is never exploding. Therefore, the gradient is strongly attenuated, since the attention weights  $a_{js}$  are tiny for most visual tokens  $s$  (Esmaeilkhani & Latecki, 2025). Layer-wise visual attention analysis is provided in appendix.

## 5. Experimental Evaluation

The main benefit of finetuning with LLL is a huge increase in the quality of Logit Lens object confidence maps, as demonstrated visually in Fig. 2. The second column shows the maps of the base model, the third NTP, and the fourth NTP+LLL finetuned. We are going from a sparse and confusing signal to sharper and precisely localized object confidence maps, which clearly demonstrate the beneficial impact of LLL on Logit Lens visualization of referred objects.

In the first two rows, although the scene within the image is cluttered, the model still successfully localizes the book and the cake, despite many distracting background details. Similarly, in rows three and four, when the object text token changes from dog to cat, the deep embeddings clearly reflect this shift: the patches corresponding to the cat appear brighter, indicating that the model effectively distinguishes between the two objects.

### 5.1. Referring Expression Segmentation

In order to quantify the quality of generated Logit Lens object confidence maps, we consider the task of referring expression segmentation in Table 1. We obtain segmentation masks either by thresholding the confidence map, or

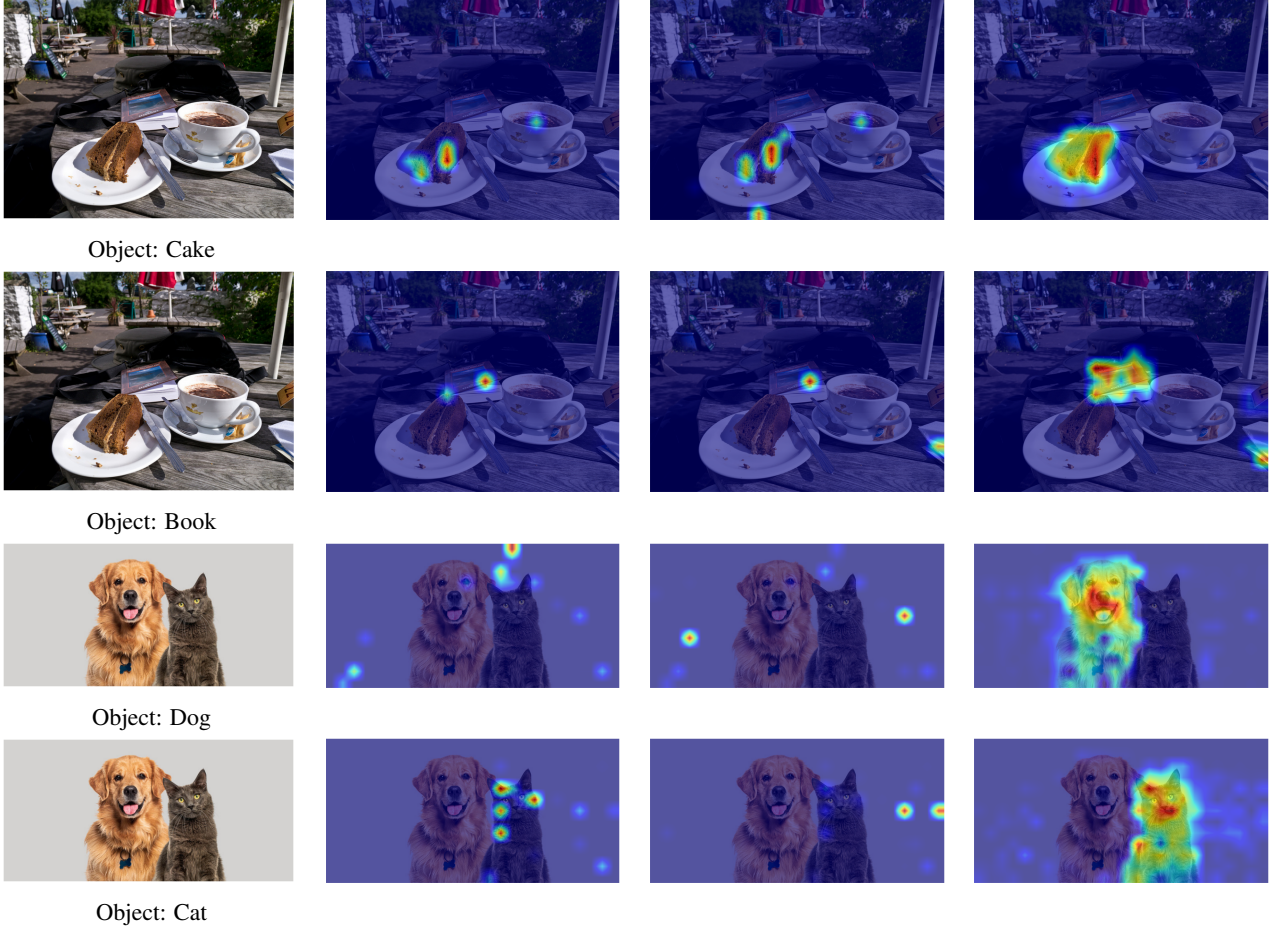


Figure 2. Logit Lens object confidence maps produced by Qwen2.5-VL-7B. First column: input image with the queried object text; second: base model; third: NTP-finetuned; fourth: NTP+LLL-finetuned. Compared to the base and NTP models, LLL produces sharply localized, object-aligned Logit Lens maps by preserving patch-level semantics in visual tokens despite cross-modal mixing in the LLM.

by extracting a bounding box from the map and using it to prompt a frozen segmentation model to generate a mask. The first 4 rows show the segmentation results obtained by thresholding the heat maps of the Logit Lens. We observe a huge improvement when Logit Lens is applied after finetuning with LLL (1st vs 3rd row). Moreover, if the results of the 3rd row are postprocessed with frozen SAM (Kirillov et al., 2023), we obtain results comparable to SOTA (4th row).

We evaluate on the referring expression segmentation (RES) task using the RefCOCO, RefCOCO+, and RefCOCOg datasets (Yu et al., 2016). All three are built on MS COCO images and require the model to localize the object referred to by a natural language description. RefCOCO focuses on short, interactive expressions, RefCOCO+ excludes absolute spatial terms, and RefCOCOg contains longer, more descriptive referring phrases. We train on the training splits and report results on the validation sets following the standard protocol.

Table 1. Referring Expression Segmentation results of supervised and training-free VLM-based methods in cloU (%). SAM indicates that a frozen SAM is used to generate masks.

Method	RefCOCO	RefCOCO+	RefCOCOg
<i>Logit Lens on Qwen2.5-VL-7B-Instr.</i>			
Base Model (Jiang et al., 2025)	63.2	52.4	53.2
NTP	65.1	53.7	54.5
NTP + LLL	71.2	63.1	65.9
NTP + LLL + SAM	<b>80.1</b>	72.6	<b>74.3</b>
<i>Finetuned-based VLMs</i>			
LISA-7B (Lai et al., 2024)	74.1	62.4	66.4
GSVA-7B (Xia et al., 2024)	76.4	64.5	71.1
F-LMM-7B (Wu et al., 2025a)	75.2	63.7	67.1
LISA-13B (Lai et al., 2024)	73.4	62.3	68.2
GSVA-13B (Xia et al., 2024)	77.7	68.0	73.2
GLaMM (Rasheed et al., 2024)	79.5	<b>75.9</b>	<b>76.8</b>
PSALM (Zhang et al., 2024)	<b>83.6</b>	<b>72.9</b>	73.8

## 5.2. POPE: Polling-based Object Probing

POPE (Li et al., 2023b) was originally designed to make the VQA evaluation fair and simple. It evaluates VLMs using binary “yes/no” object queries instead of caption generation. Each question follows the schema “Is there a <object> in the image?”, with balanced “Yes/No” answers for present and non-present objects. Finetuning and evaluation follow the protocol in POPE (Li et al., 2023b). We evaluate on the Popular Sampling split of POPE (3,000 samples). For training, we use MS COCO 2014 images with objects sampled from the 80 classes, selecting images with at least three objects and generating two “Yes” and two “No” questions per image ( $\approx 160k$  pairs).

As demonstrated in Table 2, finetuning with LLL in addition to NTP increased the accuracy of “Yes/No” answers on POPE dataset. POPE accuracy measure was introduced in (Li et al., 2023b) as a measure of hallucinations, where the higher accuracy means fewer hallucinations. So, better accuracy coincides with a reduction in object hallucinations and, consequently, better performance on VQA tasks.

*Table 2.* Performance comparison on the POPE based on Popular sampling from MSCOCO images. Higher accuracy indicates fewer hallucinated object predictions. RefCOCO  $\rightarrow$  POPE denotes zero-shot transfer: models are trained only on RefCOCO and evaluated on POPE.

Method	Accuracy (%)
<i>LLaVA-v1.5-7B</i>	
Base Model	86.23%
NTP	90.03%
NTP + LLL	92.40%
<i>Qwen2.5-VL-7B-Instr.</i>	
Base Model	86.77%
NTP	90.50%
NTP + LLL	93.87%
<i>Qwen2.5-VL-7B-Instr. (RefCOCO <math>\rightarrow</math> POPE)</i>	
NTP	86.30%
NTP + LLL	87.90%
<i>SOTA</i>	
SPIN(LLaVA-v1.5-13B) (Sarkar et al., 2025)	88.83%
VCD(LLaVA-v1.5-13B) (Leng et al., 2024)	85.74%

Importantly, **LLL improves accuracy even when the model is finetuned only on RefCOCO and evaluated directly on POPE (RefCOCO  $\rightarrow$  POPE)**, while NTP-only finetuning reduces accuracy relative to the base model, showing that LLL counteracts grounding degradation and enables cross-task generalization.

## 5.3. Logit Lens Object Confidence Scores

To qualitatively measure the impact of LLL on object localization, we consider the ratio of the average object bounding box Logit Lens score to the average score over the whole image as also used in (Choe et al., 2020; Jung & Oh, 2021). We call it the object confidence ratio.

As demonstrated by the bar plots in Fig. 3, the addition of

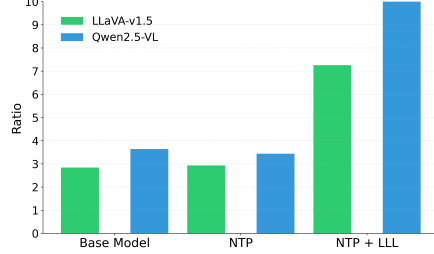


*Figure 3.* Bar plots illustrating the ratio of the object confidence scores of objects present in images within their bounding boxes to the confidence measure of the same objects averaged across all visual tokens.

LLL to NTP leads to a threefold increase in object confidence score ratio. This significant result confirms the huge impact on LLL on the object confidence maps shown in Fig. 2. Moreover, the fact that NTP did not improve the ratio confirms the fact that NTP provides only a weak supervisory signal for visual cues during fine-tuning. The results were obtained after finetuning on POPE.

## 5.4. Attention after finetuning on POPE

Interestingly, adding LLL to NTP also improves the attention of answer tokens to the correct image regions, even though LLL does not explicitly supervise attention. We measure the ratio of the last answer token’s attention to visual tokens inside the object bounding box versus all image tokens (Fig. 4); values above 1 indicate correct spatial focus. Only the NTP+LLL model exceeds this threshold, showing that object-region tokens exert stronger influence on the generated answer. This is notable since no attention-sink mitigation is applied (Kang et al., 2025). Fig. 5 visualizes this effect; sink tokens appear in the top-left, and the answer token is <yes> for the selected samples.

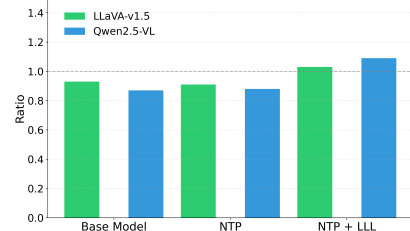


*Figure 4.* Bar plots illustrating the ratio of the average attention of target tokens within the bounding box of the target object w.r.t. the answer token to the average attention across all visual tokens.

## 5.5. Zero-Shot Pointing to Object Centers

We show that the model finetuned with NTP + LLL on RefCOCO is able to improve performance on a new localization task on a new set of images. We constructed a subset of 1,500 images from PixMo-Points (Deitke et al., 2025) for evaluation. We randomly sample from 150 object categories with the highest occurrence frequency. We stress that the images in PixMo-Points dataset have no known overlap with MS COCO. Each sample provides a short textual prompt and a human-annotated point marking the object’s center.



(a) Out-of-the-box      (b) NTP      (c) NTP + LLL

Figure 5. Attention maps of the last output token with respect to visual tokens under different settings. Queried object is “Cake”.

The model must output the corresponding  $(x, y)$  coordinates of the referred object’s center in the pixel space.

Table 3 presents zero-shot evaluation results on the PixMo-Points subset. All evaluations are performed in pixel space, with coordinates parsed from the model’s textual output using a fixed prompt template. We report the median distance in pixels. Both base models, LLaVA-v1.5 and Qwen2.5-VL, show limited ability to localize object centers without grounding-oriented supervision. Incorporating LLL during fine-tuning substantially improves both models, reducing median localization error. Notably, Qwen2.5-VL with LLL achieves a lower median distance than several proprietary and task-specific baselines, and it outperforms Molmo-7B, which was trained with explicit coordinate-level supervision on PixMo. These results indicate that LLL enables strong transfer of spatial grounding learned from RefCOCO to previously unseen object categories in PixMo

More experimental results, ablations, visualizations, and additional implementation details are provided in the appendix.

Table 3. Zero-shot performance on the Pixmo. LLaVA-v1.5 and Qwen2.5-VL were finetuned on RefCOCO training set.

Method	Median Distance
<i>LLaVA-v1.5-7B</i>	
Base Model	13.60
NTP	12.95
NTP + LLL	9.21
<i>Qwen2.5-VL-7B-Instr.</i>	
Base Model	7.07
NTP	<b>6.95</b>
NTP + LLL	<b>6.30</b>
<i>SOTA</i>	
Molmo-7B-D (Deitke et al., 2025)	7.13
GPT-4o	7.07
Gemini-2.0 Flash	7.21

## 6. Related Work

Our work is focused on the dominant group of VLMs, which are instruction-tuned, autoregressive VLMs (Li et al., 2023a; Liu et al., 2023; Bai et al., 2023; Zhu et al., 2023; Lu et al., 2024). They achieve strong results on captioning (Li et al., 2023a; Wang et al., 2021), retrieval (Radford et al., 2021; Yu et al., 2022), and VQA (Alayrac et al., 2022). However,

scaling alone does not ensure faithful grounding: VLMs still hallucinate (Liu et al., 2024), underuse visual tokens (Chen et al., 2024), and exhibit attention-sink behavior (Kang et al., 2025), indicating weak patch-level supervision and drift from image content.

A major direction for improving grounding is adding localization heads and finetuning on region-annotated data. LISA (Lai et al., 2024) introduces a [SEG] token and mask decoder; F-LMM (Wu et al., 2025a) refines attention-derived masks; and GLAMM (Rasheed et al., 2024) adds a grounding encoder and pixel decoder. While effective, these methods predict boxes or masks externally and do not bind language concepts to visual tokens inside the LLM.

Logit Lens (nostalggebraist, 2020; Jiang et al., 2025) projects intermediate VLM embeddings into the vocabulary space, showing which textual concepts each layer represents. Recent work finds that these projections reveal a drift of visual embeddings toward language-dominated representations as the model mixes the two modalities (Liu et al., 2024; Chen et al., 2024; Wu et al., 2025a). The study in (Neo et al., 2025) further shows that removing visual tokens inside ground-truth regions causes a strong drop in performance, meaning that these patches contain key semantic information that can become harder to recover after this drift. To address this, most works, such as Pix2Seq and Kosmos-2 (Chen et al., 2022; Peng et al., 2023), use coordinate-based models, or global alignment models like CLIP, UNITER, and ViLBERT (Radford et al., 2021; Chen et al., 2020; Lu et al., 2019). Unlike prior work, we directly align visual tokens with textual concepts in the logit space, preserving grounding inside the LLM without architectural changes.

Visualization methods are widely used to analyze how visual encoders and VLMs interpret images. Attention-based analyses (Darcey et al., 2023; Kang et al., 2025; Liu et al., 2024) and tools such as VL-InterpreT (Aflalo et al., 2022) examine token-level behavior, while Grad-CAM (Selvaraju et al., 2019) provides gradient-based spatial cues. In this work, we rely on Logit Lens object confidence maps to measure grounding quality and to visualize how LLL strengthens the semantic alignment of visual tokens with image content.

## 7. Conclusion

We showed that visual embeddings in autoregressive VLMs often lose their localized semantics as they propagate through LLM layers, and that next-token prediction alone does not prevent this drift. To address this, we introduced Logit Lens Loss (LLL), a lightweight auxiliary objective that aligns visual tokens with vocabulary concepts describing their image regions without architectural changes, producing sharper Logit Lens confidence maps and improving performance on vision-centric benchmarks.

## Impact Statement

Explainability is important in understanding the predictions of deep learning models. Logit Lens is a commonly accepted tool for providing explainability in VLMs, but it suffers from the diffusion of localized visual information from visual to text tokens. To alleviate this problem, we propose a Logit Lens Loss. As our experimental results demonstrate, finetuning with LLL + NTP, significantly improves the quality of Logit Lens object confidence maps. Hence, the proposed work contributes to explainability of VLM predictions.

## Acknowledgments

We thank Ying Jin for help with this work. This work was partially supported by the NSF award IIS-2331768.

## References

Aflalo, E., Du, M., Tseng, S.-Y., Liu, Y., Wu, C., Duan, N., and Lal, V. Vi-interpret: An interactive visualization tool for interpreting vision-language transformers, 2022. URL <https://arxiv.org/abs/2203.17247>.

Alayrac, J.-B., Donahue, J., Luc, P., Miech, A., Barr, I., Hasson, Y., Lenc, K., Mensch, A., Millican, K., Reynolds, M., et al. Flamingo: a visual language model for few-shot learning. In *Advances in Neural Information Processing Systems*, volume 35, pp. 23716–23736, 2022.

Bai, J., Bai, S., Yang, S., Wang, S., Tan, S., Wang, P., Lin, J., Zhou, C., and Zhou, J. Qwen-vl: A versatile vision-language model for understanding, localization, text reading, and beyond, 2023. URL <https://arxiv.org/abs/2308.12966>.

Bai, S., Chen, K., Liu, X., Wang, J., Ge, W., Song, S., Dang, K., Wang, P., Wang, S., Tang, J., et al. Qwen2. 5-vl technical report. *arXiv preprint arXiv:2502.13923*, 2025.

Chen, L., Zhao, H., Liu, T., Bai, S., Lin, J., Zhou, C., and Chang, B. An image is worth 1/2 tokens after layer 2: Plug-and-play inference acceleration for large vision-language models, 2024.

Chen, T., Saxena, S., Li, L., Fleet, D. J., and Hinton, G. Pix2seq: A language modeling framework for object detection. In *ICLR*, 2022.

Chen, Y.-C., Li, L., Yu, L., El Kholy, A., Ahmed, F., Gan, Z., Cheng, Y., and Liu, J. Uniter: Universal image-text representation learning. In *European conference on computer vision*, pp. 104–120. Springer, 2020.

Choe, J., Oh, S. J., Lee, S., Chun, S., Akata, Z., and Shim, H. Evaluating weakly supervised object localization meth-ods right, 2020. URL <https://arxiv.org/abs/2001.07437>.

Darcet, T., Oquab, M., Mairal, J., and Bojanowski, P. Vision transformers need registers. *arXiv preprint arXiv:2309.16588*, 2023.

Deitke, M., Clark, C., Lee, S., Tripathi, R., Yang, Y., Park, J. S., Salehi, M., Muennighoff, N., Lo, K., Soldaini, L., et al. Molmo and pixmo: Open weights and open data for state-of-the-art vision-language models. In *Proceedings of the Computer Vision and Pattern Recognition Conference*, pp. 91–104, 2025.

Esmaeilkhani, P. and Latecki, L. J. Direct visual grounding by directing attention of visual tokens, 2025. URL <https://arxiv.org/abs/2511.12738>.

Fu, S., Bonnen, T., Guillory, D., and Darrell, T. Hidden in plain sight: Vlms overlook their visual representations. *arXiv preprint arXiv:2506.08008*, 2025.

Jiang, N., Kachinthaya, A., Petryk, S., and Gandelsman, Y. Interpreting and editing vision-language representations to mitigate hallucinations. In *ICLR*, 2025.

Jung, H. and Oh, Y. Towards better explanations of class activation mapping, 2021. URL <https://arxiv.org/abs/2102.05228>.

Kaduri, O., Bagon, S., and Dekel, T. What’s in the image? a deep-dive into the vision of vision language models. In *CVPR*, 2025.

Kang, S., Kim, J., Kim, J., and Hwang, S. J. See what you are told: Visual attention sink in large multimodal models. In *ICLR*, 2025.

Kirillov, A., Mintun, E., Ravi, N., Mao, H., Rolland, L., Schmidt, D., Li, Z., Dollár, P., and Girshick, R. Segment anything. In *ICCV*, 2023.

Lai, X., Tian, Z., Chen, Y., Li, Y., Yuan, Y., Liu, S., and Jia, J. Lisa: Reasoning segmentation via large language model. In *Proceedings of the IEEE/CVF Conference on Computer Vision and Pattern Recognition*, pp. 9579–9589, 2024.

Leng, S., Zhang, H., Chen, G., Li, X., Lu, S., Miao, C., and Bing, L. Mitigating object hallucinations in large vision-language models through visual contrastive decoding. In *Proceedings of the IEEE/CVF Conference on Computer Vision and Pattern Recognition*, pp. 13872–13882, 2024.

Li, J., Li, D., Savarese, S., and Hoi, S. Blip-2: Bootstrapping language-image pre-training with frozen image encoders and large language models. In *International conference on machine learning*, pp. 19730–19742. PMLR, 2023a.

Li, Y., Du, Y., Zhou, K., Wang, J., Zhao, W. X., and Wen, J.-R. Evaluating object hallucination in large vision-language models. In *Conference on Empirical Methods in Natural Language Processing (EMNLP)*, 2023b.

Liu, H., Li, C., Wu, Q., and Lee, Y. J. Visual instruction tuning. *Advances in neural information processing systems*, 36:34892–34916, 2023.

Liu, S., Zheng, K., and Chen, W. Paying more attention to image: A training-free method for alleviating hallucination in l1lms. In *European Conference on Computer Vision*, pp. 125–140. Springer, 2024.

Lu, H., Liu, W., Zhang, B., Wang, B., Dong, K., Liu, B., Sun, J., Ren, T., Li, Z., Yang, H., et al. Deepseek-vl: towards real-world vision-language understanding. *arXiv preprint arXiv:2403.05525*, 2024.

Lu, J., Batra, D., Parikh, D., and Lee, S. Vilbert: Pre-training task-agnostic visiolinguistic representations for vision-and-language tasks. *Advances in neural information processing systems*, 32, 2019.

Neo, C., Ong, L., Torr, P., Geva, M., Krueger, D., and Barez, F. Towards interpreting visual information processing in vision-language models, 2025. URL <https://arxiv.org/abs/2410.07149>.

nostalgebraist. Interpreting gpt: The logit lens. <https://www.lesswrong.com/posts/AcKRB8wDpdaN6v6ru/interpreting-gpt-the-logit-lens>, aug 2020. LessWrong.

Peng, Z., Wang, W., Dong, L., Hao, Y., Huang, S., Ma, S., and Wei, F. Kosmos-2: Grounding multimodal large language models to the world. In *ICLR*, 2023.

Radford, A., Kim, J. W., Hallacy, C., Ramesh, A., Goh, G., Agarwal, S., Sastry, G., Askell, A., Mishkin, P., Clark, J., et al. Learning transferable visual models from natural language supervision. In *International conference on machine learning*, pp. 8748–8763. PMLR, 2021.

Rasheed, H., Maaz, M., Shaji, S., Shaker, A., Khan, S., Cholakkal, H., Anwer, R. M., Xing, E., Yang, M.-H., and Khan, F. S. Glamm: Pixel grounding large multimodal model. In *Proceedings of the IEEE/CVF Conference on Computer Vision and Pattern Recognition*, pp. 13009–13018, 2024.

Sarkar, S., Che, Y., Gavin, A., Beerel, P. A., and Kundu, S. Mitigating hallucinations in vision-language models through image-guided head suppression. In *Proceedings of the 2025 Conference on Empirical Methods in Natural Language Processing*, pp. 12492–12511, 2025.

Selvaraju, R. R., Cogswell, M., Das, A., Vedantam, R., Parikh, D., and Batra, D. Grad-cam: Visual explanations from deep networks via gradient-based localization. *International Journal of Computer Vision*, 128(2):336–359, October 2019. ISSN 1573-1405. doi: 10.1007/s11263-019-01228-7. URL <http://dx.doi.org/10.1007/s11263-019-01228-7>.

Tong, P., Brown, E., Wu, P., Woo, S., IYER, A. J. V., Akula, S. C., Yang, S., Yang, J., Middepogu, M., Wang, Z., et al. Cambrian-1: A fully open, vision-centric exploration of multimodal llms. *Advances in Neural Information Processing Systems*, 37:87310–87356, 2024.

Wang, C., Chen, X., Zhang, N., Tian, B., Xu, H., Deng, S., and Chen, H. Mllm can see? dynamic correction decoding for hallucination mitigation. *arXiv preprint arXiv:2410.11779*, 2024.

Wang, Z., Yu, J., Yu, A. W., Dai, Z., Tsvetkov, Y., and Cao, Y. Simvlm: Simple visual language model pretraining with weak supervision. *arXiv preprint arXiv:2108.10904*, 2021.

Wu, S., Jin, S., Zhang, W., Xu, L., Liu, W., Li, W., and Loy, C. C. F-lmm: Grounding frozen large multimodal models. In *Proceedings of the Computer Vision and Pattern Recognition Conference*, pp. 24710–24721, 2025a.

Wu, S., Jin, S., Zhang, W., Xu, L., Liu, W., Li, W., and Loy, C. C. F-lmm: Grounding frozen large multimodal models, 2025b. URL <https://arxiv.org/abs/2406.05821>.

Xia, Z., Han, D., Han, Y., Pan, X., Song, S., and Huang, G. Gsva: Generalized segmentation via multimodal large language models, 2024. URL <https://arxiv.org/abs/2312.10103>.

Xiao, L., Yang, X., Lan, X., Wang, Y., and Xu, C. Towards visual grounding: A survey. *arXiv preprint arXiv:2412.20206*, 2024.

Yu, J., Wang, Z., Vasudevan, V., Yeung, L., Seyedhosseini, M., and Wu, Y. Coca: Contrastive captioners are image-text foundation models. *arXiv preprint arXiv:2205.01917*, 2022.

Yu, L., Poirson, P., Yang, S., Berg, A. C., and Berg, T. L. Modeling context in referring expressions. In *European conference on computer vision*, pp. 69–85. Springer, 2016.

Zhang, Z., Ma, Y., Zhang, E., and Bai, X. Psalm: Pixelwise segmentation with large multi-modal model. In *European Conference on Computer Vision*, pp. 74–91. Springer, 2024.

Zhu, D., Chen, J., Shen, X., Li, X., and Elhoseiny, M.  
Minigpt-4: Enhancing vision-language understanding  
with advanced large language models. *arXiv preprint*  
*arXiv:2304.10592*, 2023.